Charge mechanism of low-frequency stimulated Raman scattering on viruses

V. B. Oshurko,[1,2,*] O. V. Karpova,[3] M. A. Davydov,[1] A. N. Fedorov,[1] A. F. Bunkin,[1] S. M. Pershin,[1] and M. Y. Grishin[1]

[1]*Prokhorov General Physics Institute of the Russian Academy of Sciences, 119991 Moscow, Russia*

[2]*Moscow State Technological University Stankin, 127055 Moscow, Russia*

[3]*Lomonosov Moscow State University, 119991 Moscow, Russia*

(Received 14 July 2021; accepted 30 March 2022; published 18 April 2022)

A physical mechanism of stimulated light scattering on nanoscale objects in a water suspension is proposed. The proposed mechanism is based on the dipole interaction between the light wave and the inevitable uncompensated electrical charge on a nanoscale object (e.g., a virus or nanoparticle) in a water environment. Experimental data on the tobacco mosaic virus are presented to support the proposed physical mechanism. It is demonstrated that stimulated amplification spectral line frequencies observed experimentally are well explained by the proposed mechanism. In particular, the absence of lower-frequency lines and the shifting of generation lines when the pH changes are due to ion friction in the ionic solution environment. The selection rules observed experimentally also confirm the dipole interaction type. It is shown that microwave radiation on the nanoscale object acoustic vibrations frequency should appear under such scattering conditions. We demonstrate that such conditions also allow for local selective heating of nanoscale objects from dozens to hundreds of degrees Celsius. This effect is controlled by the optical irradiation parameters, and it can be used to selectively affect a specific type of virus.

DOI: 10.1103/PhysRevA.105.043513

I. INTRODUCTION

Recently, many works have been published on the direct observation of acoustic vibrational modes of nanoscale objects (viruses in particular) via low-frequency optical Raman scattering [1] and extraordinary acoustic Raman scattering [2,3]. However, these techniques are limited to the study of single particles placed in artificial environments, e.g., on a surface or using double nanoholes [3], thus practical applications are also limited. The traditional electrostriction mechanism has been put forward to account for these phenomena.

There are many studies on low-frequency stimulated Raman scattering on viruses and nanoparticles in a water environment [4,5] where these objects are charged. However, there is a serious gap in the theory, namely the absence of a model for the nonlinear interaction of electromagnetic radiation with charged elastic nano-objects. In this case, a much stronger excitation mechanism than electrostriction can be responsible for this phenomenon. This mechanism is based on the interaction of a charge with an electromagnetic wave. The origin of the mechanism is in some features close to the Langmuir wave mechanism. Ultimately, this mechanism explains several ambiguous features of this type of light scattering. Presently, nanoscale biological objects such as viruses in water suspensions are of great interest [6], and obtaining new information on such objects via a new method opens up new possibilities for controlling these objects. For example, the proposed mechanism opens up the possibility of selective heating via resonant biharmonic pumping of only a specific type of virus in a suspension of various viruses.

At present, the mechanism of stimulated light scattering is not completely clear for nanoscale objects. Stimulated light scattering with a frequency shift equal to the frequency of the acoustic vibrations characteristic of nanoscale objects is traditionally explained using models based on the electrostriction (ponderomotive) mechanism, which suggests the modulation of the electric susceptibility of an electrically neutral medium by an external field [7]. The electrostriction mechanism clearly does not fit the phenomenon considered in this study because the medium is not electrically neutral in a virus suspension. Biological and nonbiological objects (e.g., viruses and polymeric nanospheres, respectively) in water suspensions have a significant uncompensated electrical charge [8,9], and the protein shell (capsid) of viruses, which is composed of amino acids, undergoes electrolytic dissociation in a water environment [10]. This explains the phenomenon of proteins and ribonucleic acid electrophoresis caused by uncompensated electrical charge, as the number of acid residues is different from the number of alkaline residues [10]. Consequently, proteins and viruses exhibit the so-called isoelectric point, i.e., the pH of the environment when the uncompensated charge dissipates. Therefore, the uncompensated charge value of the virus can be controlled by varying the pH of the solution.

The experimental studies in the literature show that polymeric nanospheres in water suspensions also possess a significant charge, e.g., $\sim 20e$ (elementary charges) per a single 50-nm polystyrene nanoparticle [8]. It is obvious that the energy of the electrostatic interaction between such a charge and the electric field in the laser beam waist is many orders of magnitude larger than the electrostriction interaction energy (i.e., the energy of interaction between the induced dipole moment and the external field). The electrostatic force affecting

*vadimoshurko@gmail.com

the charge is evidently much stronger than the electrostriction forces. Until now, this scenario has not been taken into account, although the interaction between the electromagnetic field of the light beam and the charge may be the primary mechanism determining the low-frequency stimulated light scattering phenomenon.

Due to ionic (or cataphoretic) friction, the presence of a significant uncompensated electrical charge causes a strong suppression of acoustic vibrations in nanoscale particles surrounded by water [8]. In other words, the friction should be so strong that any vibration is almost impossible. However, experiments show that in water suspensions of nanoparticles, including viruses, a directional stimulated emission is formed on Stokes frequency (i.e., redshifted by the value of the frequency of the acoustic vibrations inherent in these particles). We will subsequently refer to this effect as low-frequency stimulated light scattering (LFSS).

There are a series of LFSS peculiarities, which are comparable to conventional stimulated Raman scattering (SRS). For example, unlike SRS, LFSS is almost never observed on the frequency of the lowest vibrational mode [4,5,7]. Furthermore, as will be shown later, in the case of viruses, the observed LFSS frequency can depend on the ion and virus concentrations in the solution.

LFSS also differs noticeably from the stimulated Brillouin scattering (SBS) process. In SBS, the stimulated light scattering appears on an acoustic wave inside a macroscopic object, and the frequency shift is defined only by the speed of sound in this object. In LFSS, the frequency shift is clearly caused by the scattering of acoustic waves on nanoscale objects and is dependent on the characteristics of the nanoscale objects, such as size. Thus, these peculiarities and the unclear mechanism of stimulated light scattering on nanoscale objects' acoustic vibrations enable us to state that LFSS is a new nonlinear optics phenomenon. The purpose of this work is to develop a model that describes the LFSS phenomenon based on a charge mechanism and to explain the experimentally observed features of the process.

II. FORMALISM

A. Charge mechanism of LFSS

Consider a simplified model of a charged dielectric nanoscale object (a nanosphere or nanosized virus particle) in the electromagnetic field of a light wave. The object itself is not electrically neutral in this case. Usually, the excess charge of such an object is compensated for by oppositely charged ions in the solution or a surfactant, which is always added to a nanoparticle suspension to prevent adhesion. This charge-compensating ionic shell size is defined by the Debye length for the solution. The existence of such a shell requires adding another factor to the model, i.e., the friction that inevitably appears during acoustic vibrations of a nanoscale object in an ionic shell.

Let the TE light wave be directed along the z axis and the electric field vector oscillate along the x axis. The wave equation for $\boldsymbol{E}(\boldsymbol{r},t)$ is given as

$$\hat{D}\boldsymbol{E}(\boldsymbol{r},t) = \nabla(\nabla \boldsymbol{E}(\boldsymbol{r},t)) + \frac{4\pi}{c^2}\frac{\partial \boldsymbol{J}(\boldsymbol{r},t)}{\partial t}, \tag{1}$$

where $\hat{D} = \Delta - 1/c^2\partial^2/\partial t^2$ is the d'Alembertian, c is the speed of light, and $\boldsymbol{J}(\boldsymbol{r},t)$ is the density of the current induced by the acoustic movement of the charge. In the case of usual SRS or the electrostrictional (ponderomotive) mechanism, the first term on the right-hand side of the equation is equal to zero because of the zero total charge of the medium. However, in our case we should take into account that

$$\nabla \boldsymbol{E}(\boldsymbol{r},t) = 4\pi q(\boldsymbol{r},t),$$

where $q(\boldsymbol{r},t)$ is the charge volume density.

Let the object be charged uniformly with the initial charge density constant over the volume ($q_0 = \text{const}$). If the object is absolutely rigid (i.e., its elastic modulus equals infinity), there will be no movement apart from reciprocating oscillations in the field $\vec{E}$ of the light wave. Such oscillations make no contribution to inelastic light scattering and will not be considered. Acoustic vibrations are possible in an elastic object with a finite Young's modulus, and they can appear spontaneously at room temperature because the acoustic phonon energy $h\Omega$ is much less than the heat energy k_BT.

Let us consider the acoustic displacement $\boldsymbol{u} = \boldsymbol{r}' - \boldsymbol{r}$, where $\boldsymbol{r}'$ is the displaced position of point $\boldsymbol{r}$ in an acoustic wave. The solid body acoustic equation can be expressed as

$$\Delta u(r,t) - \Gamma\frac{\partial \boldsymbol{u}(\boldsymbol{r},t)}{\partial t} - \frac{1}{v^2}\frac{\partial^2 \boldsymbol{u}(\boldsymbol{r},t)}{\partial t^2} = \frac{1}{v^2}\boldsymbol{F}_m, \tag{2}$$

where v is the speed of sound, and $\boldsymbol{F}_m$ is the force mass density, i.e., volume density ($\boldsymbol{F}_v = d\boldsymbol{F}/dV$) divided by the density of the mass, $\boldsymbol{F}_m = \boldsymbol{F}_v/\rho$. Here, we also introduce the phenomenological term that describes the friction proportional to velocity with the coefficient Γ. As was mentioned earlier, this is necessary to account for external ionic shell resistance to oscillations.

It is obvious that in our case, the force density is

$$\boldsymbol{F}_m = q(\boldsymbol{r},t)/\rho(\boldsymbol{r},t)\boldsymbol{E}(\boldsymbol{r},t),$$

where q is the charge volume density.

An acoustic wave in a nanoscale object can be naturally considered as a wave of density modulation $\rho'(\boldsymbol{r},t) = \rho_0 f(\boldsymbol{r},t)$, where f is the dimensionless function describing this wave. The charge density modulation is described by the same function f, and consequently the ratio q'/ρ' on the right-hand side of Eq. (2) remains constant.

Then the only form of direct interaction between the light wave field and the nanoscale object charge is *charge decompensation* caused by the well-known Debye-Falkenhagen effect [11]. When an electromagnetic wave passes through an ionic solution, starting from a wave frequency, the ion *heavy* hydration shell fails to *keep up* with the ion movement, leading to a sharp growth in solution conductivity. For the majority of water solutions, this frequency lies in the region of several gigahertz and is lower than the observed characteristic frequencies of nanosphere/virus acoustic vibrations (dozens of gigahertz). In recent works, the inertia of hydration shells is always taken into account [12] in explaining the emergence of uncompensated charge while exciting acoustic vibrations in charged nanoscale objects.

The origin of the *charge decompensation* wave is close to the well-known Langmuir waves in plasma [13]. However, these waves are not identical to Langmuir's wave. In

plasma, the charges are practically free and the elasticity of the "oscillator" is determined only by the Coulomb interactions. In a virus, charges are bound to the surface of a large (300 nm) rigid body—the virus capsid. In this case, the elasticity of the oscillator (and also its eigenfrequency) is determined by Young's modulus of the capsid proteins.

For simplicity, consider a one-dimensional problem describing a tobacco mosaic virus particle that looks like a thin cylinder. Like the light wave E vector, let the cylinder axis be directed along the x axis. If the negative (or positive) charge volume density of the virus is modulated by an acoustic wave $q^-(x,t) = q_0^- f(x,t)$, then the opposite ion charge density in the hydration shell in the solution remains constant ($q^+ = q_0^+$) due to the Debye-Falkenhagen effect, and it equals q_0 for the one-dimensional problem. The total charge density is then defined by the difference $q(x,t) = q_0^- f(x,t) - q_0^+$. An easy direct calculation shows that the total charge density is $q(x,t) = q_0 \frac{\partial u}{\partial x}$.

Apart from the force induced by the light wave field $q_0 u_x E(z,t)$, there are also interactive forces between charged areas similar to that in Langmuir waves in plasma. These forces are

$$F_e = q(x,t)E' = q(x,t)\int \frac{\partial E'}{\partial x}dx = q(x,t)\int 4\pi q(x,t)dx = 4\pi q_0^2 u u_x, \tag{3}$$

where E' is the field created by uncompensated charges.

Finally, the equation for acoustic displacement $u(x,t)$ is

$$u_{xx} - \Gamma u_t - \frac{1}{v^2}u_{tt} = \frac{q_0}{\rho_0 v^2}u_x E(z,t) + 4\pi\frac{q_0^2}{\rho_0 v^2}u u_x. \tag{4}$$

B. Dipole approximation

It is difficult to find a general solution of this equation for a harmonic light wave. However, it is evident that a charge moving in the field of a light wave does not itself cause inelastic scattering. To find the inelastic components of the scattering, it is necessary to examine the processes in which the light wave field modulates a parameter of the system. In particular, let us consider the modulation of the total dipole moment by the external electric field. To achieve this, an auxiliary problem has to be solved: consider a constant force affecting the dipole moment of the object instead of a light wave field, i.e., let us determine how a constant external field changes the dipole moment.

On the right side of Eq. (4), there is the density of the force affecting the object via the field and the interaction between the areas of the distributed charge. The estimation readily shows that although the LFSS field is relatively weak compared to the left side of Eq. (4), the second term on the right side of Eq. (4) (the interaction between the areas) is much smaller than the first term for realistic acoustic vibration amplitudes and can thus be neglected.

It is obvious that in the absence of acoustic vibrations, the charge distribution is uniform and there is no dipole moment—or, to be precise, it is possible to choose a reference frame in which the dipole moment equals zero. The dependence of a charged object dipole moment on the chosen reference frame is insignificant as force is defined only by the dipole moment derivative. When an acoustic wave appears, charged areas are created due to charge decompensation, and the total dipole moment (per unit volume) for a virus of length L and its derivative are

$$p = \frac{q_0}{L}\int_0^L x u_x dx \tag{5}$$

and

$$p_x = \frac{q_0}{L}L u_x(L) = q_0 u_x(L).$$

In a dipole approximation, to determine the force affecting each element dx at point x, we determine the coordinate-dependent dipole moment $p(x)$ and its derivative as

$$p_x(x) = q_0 u_x.$$

The light wave electric field force density is

$$F_v = \tfrac{1}{2}p_x E(z,t) = \tfrac{1}{2}q_0 u_x E(z,t). \tag{6}$$

Estimations show that the magnitude of the dipole moment and the force affecting the dipole are in fact much larger than the electrostriction (ponderomotive) forces traditionally considered in nonlinear optics.

In Eqs. (5) and (6), the displacement $u(x,t)$, and consequently the dipole moment, are functions of the external field E. To consider the dependence $p(E)$ using the simplified model, let us examine a charged object (a virus) in a constant external field E. As $E = \text{const}$ on the right-hand side of Eq. (4), using the standard substitution $u(x,t) = U(t)V(x)$, we derive the following system of equations:

$$U_{tt}(t) + \gamma U_t(t) + \Omega_m^2 U(t) = 0, \tag{7}$$

$$V_{xx}(x) - \frac{q_0}{2\rho_0 v^2}E V_x(x) + \frac{\Omega_m^2}{v^2}V(x) = 0. \tag{8}$$

Here, we denote $\gamma = \Gamma v^2$ and the common constant $-\Omega_m^2/v^2$. The solution of Eq. (8), with the free ends condition $u_x(0) = u_x(L) = 0$, is

$$V(x) = u_0 e^{\frac{q_0 E x}{4\rho_0 v^2}}\cos\left(x\sqrt{\frac{{\Omega_m}^2}{v^2} - \frac{E^2 {q_0}^2}{16{\rho_0}^2 v^4}}\right), \tag{9}$$

where $\Omega_m = m\pi v/L$ is the mth mode eigenfrequency, and u_0 is the amplitude. Hence, we can determine the derivative of the dipole moment based on Eqs. (5), (6), and (9),

$$p_x(E) = U(t)\frac{u_0 q_0}{4\rho_0 v^2}e^{\frac{q_0 E L}{4\rho_0 v^2}} \times [q_0 E\cos(\Omega_E L) - (4v^2\rho_0\Omega_E)\sin(\Omega_E L)], \tag{10}$$

where

$$\Omega_E = \sqrt{\frac{\Omega_m^2}{v^2} - \frac{E^2 {q_0}^2}{16\rho_0^2 v^4}}. \tag{11}$$

In Eqs. (10) and (11), $U(t)$ is the solution of Eq. (7) in the form of a periodic function with $\sqrt{\Omega_m^2 - \gamma^2}$ frequency and the attenuation coefficient γ. For our purposes, let $U = 1$.

In Eqs. (7) and (8), the field E is constant, and Eqs. (7), (8), and (9) are not intended to solve the stimulated amplification problem but are only used to estimate the dipole moment dependence on the field.

Under the conditions of LFSS, the field can be considered small, i.e., $E \ll 4\rho_0\Omega_m v/q_0$. This is true up to $E \sim 10^9$ V/m, which is significantly stronger than the intensities used in experiments, i.e., $I \sim 1$ MW/cm^2. Thus, $p_x(E)$ can be expanded into a series using E,

$$p_x(E) = \frac{q_0^2 u_0 (-1)^m}{2\rho_0 v^2} E + \frac{3}{16}\frac{q_0^3 u_0 L (-1)^m}{\rho_0^2 v^4} E^2 + \ldots. \quad (12)$$

The series coefficients depend on the amplitude of the initial oscillation u_0, which is quite different in regular molecular SRS. In fact, almost any molecule has nonzero polarizability; however, in our case, the polarizability is not equal to zero only if the initial charge distribution is nonuniform. This is possible, for example, due to spontaneous acoustic vibrations. If there is no nonuniform distribution, then the polarizability (i.e., the dipole moment dependence on the external field) evidently equals zero. The external field itself affects all areas equally, and hence it does not create a nonuniform charge distribution, which would result in a nonzero dipole moment.

C. Stimulated amplification of radiation

Given the dipole approximation, we substitute the force density with $1/2 p_x[E(z,t)]E(z,t)$ on the right-hand side of the acoustic equation, Eq. (4). Accounting for the expansion of Eq. (12), for the first two terms of the series we obtain

$$u_{xx} - \Gamma u_t - \frac{1}{v^2} u_{tt} = \alpha_1 E(z,t)^2 + \alpha_2 E(z,t)^3, \quad (13)$$

where

$$\alpha_1 = \frac{q_0^2 u_0 (-1)^m}{4\rho_0 v^2}, \quad \alpha_2 = \frac{3 q_0^3 u_0 L (-1)^m}{32 \rho_0^2 v^4} \quad (14)$$

and $E(z,t)$ is the light field. To determine the amplification of the radiation components in a stimulated process, we consider a combination of a pump wave and a Stokes wave based on the traditional nonlinear optics approach $E(z,t) = E_0 \exp(i\omega_0 t - ik_0 z) + E_s \exp(i\omega_s t - ik_s z) + \text{c.c.}$ In this case, the right side of Eq. (13) does not depend on x, and Eq. (13) can be split into two ordinary equations,

$$U_{tt}(t) + \gamma U_t(t) + \Omega_m^2 U(t) = \alpha_1 E(z,t)^2 + \alpha_2 E(z,t)^3 \quad (15)$$

and

$$V_{xx}(x) + \frac{\Omega_m^2}{v^2} V(x) = 0. \quad (16)$$

The second equation, Eq. (16), with the free ends condition is an expression for eigenfrequencies $\Omega_m = \frac{m\pi v}{L}$, $m = 1, 2, \ldots,$

$$V(x) = u_0 \cos\left(\frac{\Omega_m}{v} x\right). \quad (17)$$

In the first equation, Eq. (15), we substitute the combination of pump and Stokes waves (frequencies ω_0 and ω_s, respectively) mentioned earlier, and we derive a solution $u = UV$ at a frequency $\Omega = \omega_0 - \omega_s$,

$$u_\Omega = \alpha_1 V(x) \frac{E_0 E_s}{\Omega_m^2 - \Omega^2 + 2i\gamma\Omega} e^{(i\Omega t - ik_\Omega z)}. \quad (18)$$

Similarly, we derive a solution at the Stokes frequency ω_s,

$$u_s = \alpha_2 V(x) \frac{E_0^2 E_s}{\Omega_m^2 - \omega_s^2 + 2i\gamma\omega_s} e^{(i\omega_s t - ik_s z)} \quad (19)$$

It can be seen that the second solution for the Stokes component ω_s does not have pronounced resonances at detuning equal to eigenfrequencies $\omega_0 - \omega_s = \Omega_m$ and does not explain the observed stimulated amplification at these frequencies.

Consequently, the only possible stimulated amplification mechanism for Stokes or anti-Stokes frequencies is a simultaneous amplification at a microwave frequency Ω (at which waves with frequencies ω_0 and ω_s are combined) and further amplification of the frequency ω_s when the frequencies ω_0 and Ω are combined.

D. Coupled waves equations

To investigate the possibility of such simultaneous amplification, we consider the propagation of four waves at the frequencies ω_0, Ω, ω_s, and ω_a (where ω_a is the anti-Stokes radiation frequency). Again, we derive the solutions of Eq. (13) for these frequencies considering only the first-order terms on the right side of the equation,

$$u_0 = \alpha_1 V(x) \frac{(E_0 E_s + E_0 E_a)}{\omega_m^2 - \omega_0^2 + 2i\gamma\omega_0} e^{(i\omega_0 t - ik_0 z)}, \quad (20)$$

$$u_s = \alpha_1 V(x) \frac{E_0 E_\Omega}{\Omega_m^2 - \omega_s^2 + 2i\gamma\omega_s} e^{(i\omega_s t - ik_s z)}, \quad (21)$$

$$u_a = \alpha_1 V(x) \frac{E_0 E_\Omega}{\Omega_m^2 - \omega_a^2 + 2i\gamma\omega_a} e^{(i\omega_a t - ik_s z)}, \quad (22)$$

$$u_\Omega = \alpha_1 V(x) \frac{(E_0 E_s + E_0 E_a)}{\Omega_m^2 - \Omega^2 + 2i\gamma\Omega} e^{(i\Omega t - ik_\Omega z)}. \quad (23)$$

Next, to substitute these equations into the wave equation, Eq. (1), we define the terms $J_t = \mu_0 \partial^2 u_i / \partial t^2$, and using a slowly varying envelope approximation, we obtain a system of coupled wave equations in which we wave out the dependence on the x coordinate,

$$\frac{dE_0}{dz} = \beta_0 E_\Omega (E_s + E_a), \quad (24)$$

$$\frac{dE_s}{dz} = \beta_s E_\Omega E_0, \quad (25)$$

$$\frac{dE_a}{dz} = \beta_a E_\Omega E_0, \quad (26)$$

$$\frac{dE_\Omega}{dz} = \beta_\Omega E_0 (E_s + E_a), \quad (27)$$

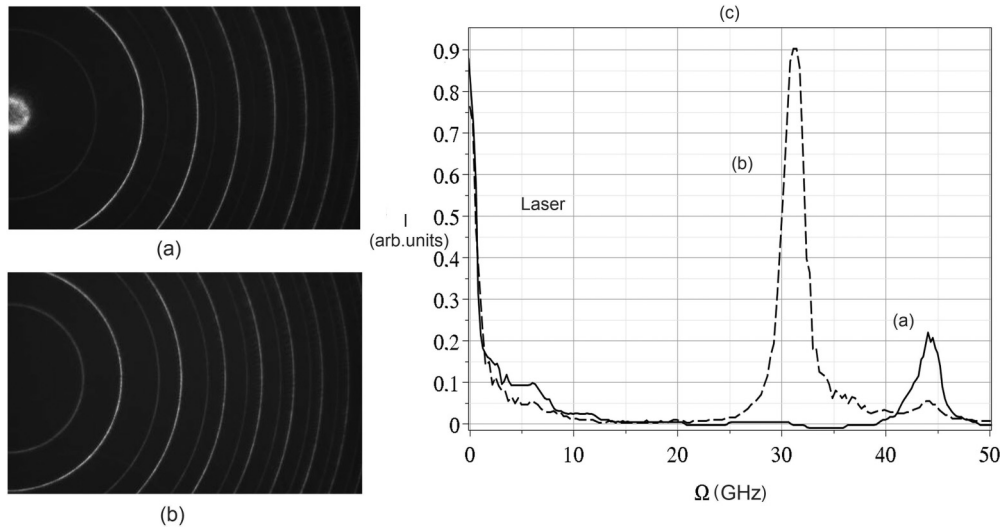

FIG. 1. Experimental low-frequency stimulated scattering: (a),(b) interference fringes from a Fabry-Pérot interferometer and (c) LFSS spectra for the tobacco mosaic virus concentration (a) $\sim 1.0 \times 10^{12}\,\mathrm{cm}^{-3}$, $\Delta\nu \sim 44.1\,\mathrm{GHz}$ and concentration (b) $\sim 2.0 \times 10^{12}\,\mathrm{cm}^{-3}$, $\Delta\nu \sim 31.38\,\mathrm{GHz}$.

where β are constants defined by Eqs. (18)–(23). Solving these equations for the Stokes component, we obtain

$$E_s(z) = \frac{E_{s0}}{1 - E_{s0}\mathrm{Re}(\chi)z}, \tag{28}$$

where E_{s0} is the magnitude of Stokes radiation (e.g., spontaneous Stokes radiation) at $z = 0$, and χ is

$$\chi(\Omega) = \sqrt{-\frac{c^2\mu_0^2\alpha_1^2\omega_0\Omega}{(\Omega_m^2 - \omega_0^2 + 2i\gamma\omega_0)(\Omega_m^2 - \Omega^2 + 2i\gamma\Omega)}}\left(\frac{(\omega_0+\Omega)\big(\Omega_m^2 - (\omega_0-\Omega)^2 + 2i\gamma(\omega_0-\Omega)\big)}{\big(\Omega_m^2 - (\omega_0+\Omega)^2 + 2i\gamma(\omega_0+\Omega)\big)(\omega_0-\Omega)} + 1\right). \tag{29}$$

III. COMPARISON OF THE THEORY WITH EXPERIMENT

We can now compare the developed theoretical model with experimental results on low-frequency stimulated light scattering in suspensions of tobacco mosaic virus (TMV) in tris buffer. As can be seen from (29), the theoretical model predicts that the dumping coefficient defines which lines are amplified. In the experiment, this coefficient can be tuned by changing the pH of the solution. The easiest way is to change the pH of the solution without changing the other experimental conditions by evaporating a part (for example, half of the water) in the vessel.

In the experimental setup described in detail in the Bunkin *et al.* study [6], the cuvette with the studied suspension was irradiated by focused second-harmonic pulses of a single-frequency YAG : Nd^{3+} laser (wavelength λ of 532 nm, pulse duration τ of 10 ns, and pulse energy E_p of up to 40 mJ). The radiation was focused onto the cuvette center by a lens with a focal length f of 30 mm. Stimulated light scattering spectra were studied using a Fabry-Pérot interferometer and recorded with a complementary metal-oxide semiconductor (CMOS) camera, a Basler acA1920-40 μm. The chosen intensity ensures that the obtained spectra are caused by stimulated Raman scattering rather than stimulated Brillouin scattering [6]. It was experimentally shown in [6] that when the intensity is so high ($\sim 10^9\,\mathrm{W/cm}^2$) stimulated Raman scattering of light dominates, and stimulated Brillouin scattering disappears. The formation of laser plasma was not observed during experiments.

The results of the TMV suspension spectra measurements [14] are presented in Fig. 1. For a virus concentration of $1.0 \times 10^{12}\ \mathrm{cm}^{-3}$ and a laser pulse energy E_p of $\sim$20 mJ, an LFSS line was detected at a $1.47\,\mathrm{cm}^{-1}$ shift relative to the pump line, which corresponds to a 44.1 GHz oscillation frequency [Fig. 1(a)]. For a virus concentration of $2.0 \times 10^{12}\ \mathrm{cm}^{-3}$ and a laser pulse energy of $\sim$30 mJ, an LFSS line was detected at a $1.046\,\mathrm{cm}^{-1}$ shift [31.38 GHz, Fig. 1(b)]. The experimental results also confirm this directional character of the LFSS emission. An electron microscopy view of a dried TMV suspension after LFSS experiments is shown in Fig. 2. No changes in the shape of viruses after irradiation have been observed.

Thus, experiment confirms changes in amplified line frequency due to a change of pH of the solution. Simple estimations (17) show that observed lines are not the lowest eigenfrequency lines.

Also, the LFSS spectra of suspensions of polystyrene nanoparticles of various diameters were measured in Ref. [15]. As for the virus suspension, lines corresponding to the lowest eigenfrequencies of polystyrene spheres were not observed in [15]. The stimulated Raman scattering lines were in the region above 10 GHz. Now this can be easily explained if we take into account the mechanism of ionic friction proposed here.

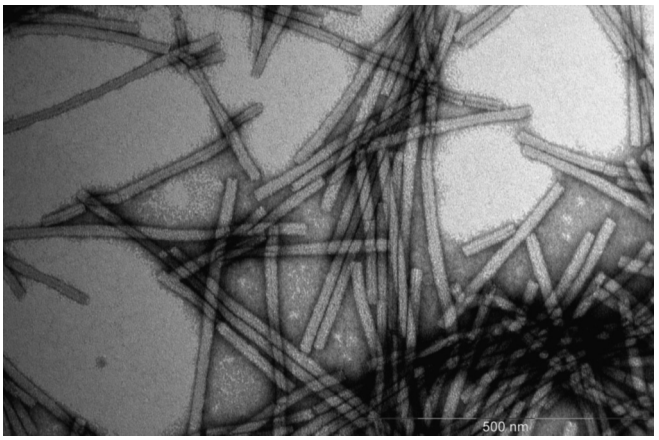

FIG. 2. Electron microscopy picture of dried TMV suspension after LFSS experiments.

A. Vibrational states selection rules

Considering the experimentally measured values of Young's modulus and the speed of sound of TMV in the study by Stephanidis *et al.* [16], it is easy to calculate acoustic vibrations frequencies for a TMV cylinder 300 nm in length and 18 nm in diameter in a water environment. Numerical calculations performed in the COMSOL MULTIPHYSICS software for all possible vibration types (supposing the speed of sound $v = 3430$ m/s, density $\rho_0 = 1100\,\mathrm{kg/m^3}$, and Young's modulus E = 9.5 MPa [6]) yield the results shown in Table I.

Bending vibration frequencies turned out to be higher than 112 GHz, and radial vibration frequencies are above 190 GHz. As can be seen, the longitudinal vibration frequencies 34 and 45 GHz coincide well with the observed TMV LFSS frequencies (31 and 44 GHz). Notably, increasing the virus concentration in tris buffer in the experiments yielded the observed LFSS frequency switch from 44 to 31 GHz. In one experimental session, the 44 and 31 GHz lines even appeared simultaneously, but the intermediate frequency, ≈40 GHz, was never observed.

This observation is in good agreement with the proposed theoretical model. In fact, the ≈40 GHz frequency corresponds to an even vibrational mode for which the integral [Eq. (5)] defining the dipole moment [Eq. (17)] equals zero. Hence, the experiment confirms the dipole type of interaction and the subsequent selection rule for odd vibrational modes.

Therefore, the absence of lower vibrational frequencies in the amplified LFSS lines can now be explained. In fact, the expression in Eq. (29) denoting the gain increment defines only one *window* of amplification. As can be seen from Eq. (29), this window is dependent on the magnitude of the ionic friction γ. Figure 3 presents the gain increment $\mathrm{Re}(\chi)$ as a function of Ω for a set of resonance odd mode frequencies Ω_m from Table I ($m = 1, 3, \ldots$) for two values of the ionic friction coefficient (2.0 and 10.0 GHz). It is evident that the weaker friction (2.0 GHz) results in a maximal gain increment $\mathrm{Re}(\chi)$ for $m = 4$ at a frequency of approximately 33 GHz. The apparent reason for this is nonzero ionic friction. The increase in ionic friction coefficient to 10.0 GHz—as expected—leads to an enormous broadening and merging of resonance peaks, with the maximum at ∼41 GHz.

TABLE I. TMV longitudinal vibration mode frequencies.

M	0	1	2	3	4	5	6	7
f (GHz)	5.71	11.43	17.15	22.86	28.58	34.30	40.01	45.73
M	8	9	10	11	12	13	14	15
f (GHz)	51.45	57.16	62.88	68.60	74.32	80.04	85.76	91.48

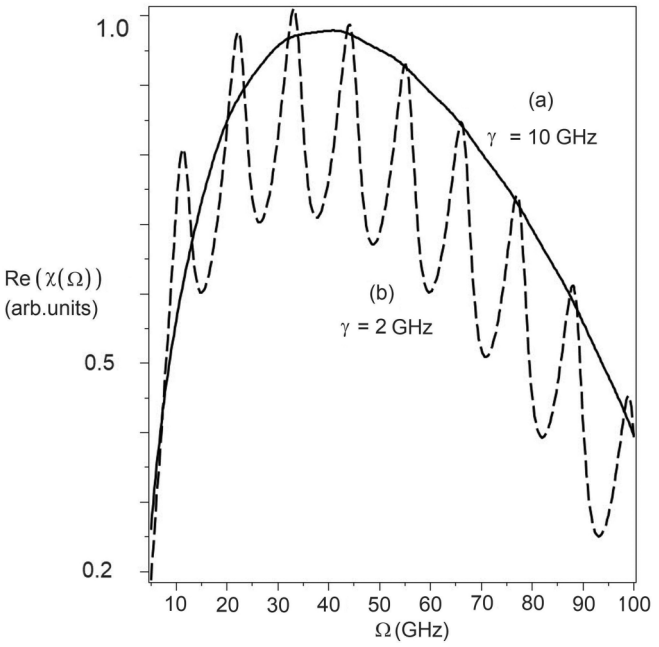

FIG. 3. Gain *increment* for the frequencies of 10 odd modes ($m = 1, 3, 5, \ldots$) from Table I for two friction coefficients: (a) 10.0 GHz (solid) and (b) 2.0 GHz (dashed).

Figure 4 illustrates the growth of these components with an increase in the interaction length z, based on Eq. (31). Upon reaching z = 2.65 mm, the spectrum is reduced to virtually a single line: the 41 GHz line for the 10.0 GHz friction coefficient, and the 33 GHz line for the 2.0 GHz friction coefficient.

These results correspond well to the experimental data and allow for explaining the observed LFSS frequency change caused by an increase in the TMV concentration in the suspension. The ionic friction evidently decreases with a decrease in the number of ions *compensating* the charge on the virus. During the experiments, we increased the virus concentration by evaporating water from the solution, but *heavy* virus particles and tris molecules, which create a weak-alkaline environment, were not evaporated. Hence, the pH of the solution increased. As mentioned earlier, the isoelectric point (i.e., the pH for which the virus becomes electrically neutral) lies at rather high pH values (i.e., high alkalinity). Therefore, as water evaporates, the pH increases and the value of the uncompensated charge decreases. Consequently, there are fewer solution ions compensating for the charge of the virus, leading to a reduction in ionic friction, which in turn results in a change in amplification frequency (Fig. 4).

Only one adjustable parameter was used to describe this LFSS phenomenon, i.e., the ionic friction magnitude. Notably,

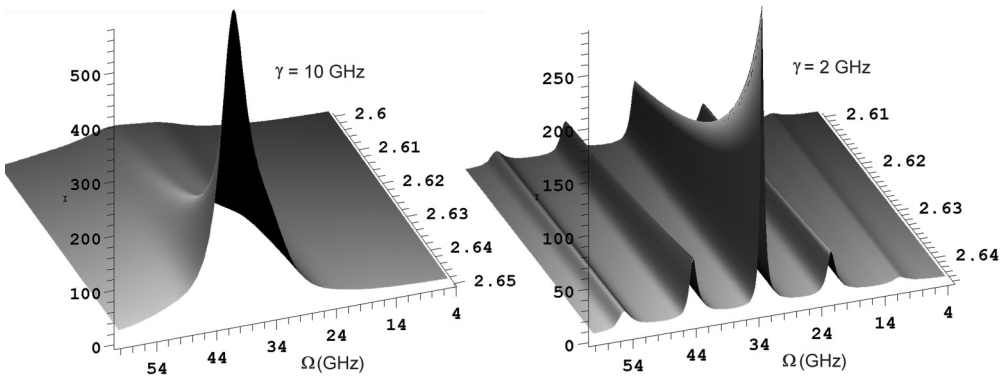

FIG. 4. Gain dependence on the interaction length z for the frequencies of 10 odd modes ($m = 1, 3, 5, \ldots$) from Table I and spectral lines at the exit from the interaction region $z = 2.65$ mm for the friction coefficients (a) 10.0 GHz, (b) 2.0 GHz.

this phenomenon can hardly be explained in terms of other physical mechanisms.

Another experimental result can now be easily understood: the experimental series in [15] reveals that for both 70 and 500 nm polystyrene particle suspensions, LFSS lines with very close frequencies are observed (i.e., 18–20 GHz), although the particle size and the lower resonant frequency differ by orders of magnitude. However, taking into account that friction does not depend on the surface area, the *window* of amplification is the same for the same friction coefficient for both cases (e.g., for *big* and *small* nanoparticles) based on Eq. (29). Furthermore, only those modes with frequencies around the amplification maximum are amplified.

B. Nanoscale objects heating

Another conclusion follows directly from the preceding conclusion. If some part of the pump energy is spent on overcoming friction, this should result in the heating of the local nanoscale particles. To roughly estimate this heating in terms of the described theoretical model, we suppose that the virus is a dipole with a moment $p \approx QL$, where Q is the uncompensated charge value experimentally estimated as $\sim 50 \times 1.6 \times 10^{19}$ C. The energy of the dipole in the field E is then $A \approx QLE$, and the total power can be taken as $P \approx QLE\Omega_m$. The portion of this power converted into heat can be estimated from the magnitude of the ionic friction as $1 - \exp(-\gamma\tau_p)$, where τ_p is the laser pulse duration. With the friction coefficient $\gamma \approx 10^9$ c^{-1} and pulse duration $\tau_p \gg 1/\gamma$, all of the absorbed radiation is transformed into heat. The amount of heat produced during the pulse τ_p is $A \approx QLE\Omega_m\tau_p$. Then, if we neglect the thermal conductivity (during the laser pulse, the heat wave diffusion length is $\sim$100 nm, given a water thermal conductivity $\chi = 1.9 \times 10^{-5}$ cm^2/s), we obtain the final heating temperature as

$$T \approx \frac{QL\Omega_m\tau_p}{\rho_0 C_p V} E_0, \tag{30}$$

where $C_p \approx 3000$ J/(kg K) is the protein heat capacity. Then, at a light field strength $E_0 \approx 10^8$ V/m, we obtain the heating as $T \approx 26.0$ K during a 10 ns laser pulse. This rough estimate shows that heating can occur in experiments, though the temperature is still insufficient to denature the proteins.

However, it is obvious that a simple severalfold pulse duration increase (up to 0.1–1 μs) may lead to a strong local heating of up to dozens or hundreds of degrees Celsius. Nevertheless, the overall heating may be insignificant in all these cases. Notably, the virus is heated by local selective nonresonant radiation that is not absorbed by the suspension. This is the stimulated nature of the process that provides highly selective heating of certain virus types.

It is known that TMV heating up to only 94°C leads to partial denaturation of capsid proteins and the formation of a spherical virus [17,18]. Therefore, selective heating of given virus types that changes the capsid shape may strongly affect the virus functioning.

It is significant that LFSS allows for selectively heating given types of nanoscale objects up to substantial temperatures. The very possibility of such heating opens new prospects for local selective treating of nanoscale objects, viruses, and cellular organelles via nonlinear optics for biomedical applications.

IV. CONCLUSION

In this work, a physical mechanism of low-frequency stimulated light scattering on nanoscale objects in water suspension is proposed. The proposed model differs significantly from the traditional stimulated scattering mechanism based on electrostriction. The model is based on a dipole interaction between the light wave and the uncompensated electrical charge that inevitably exists on a nanoscale object (virus or nanoparticle) in a water environment. The experiments were conducted by observing low-frequency stimulated light scattering in tobacco mosaic virus suspensions, and the data obtained support the proposed model. The selection rules observed experimentally also confirm the dipole type of the interaction. It has been demonstrated that stimulated amplification spectral line frequencies observed experimentally cannot be explained by traditional mechanisms but are well explained by the proposed charge mechanism. In particular, the absence of lower-frequency lines and the *window of amplification* are due to ion friction in the ionic solution environment. It has been shown that under low-frequency stimulated light scattering conditions, microwave radiation should appear at nanoscale object acoustic vibration eigenfrequency. We demonstrate that such conditions also allow for local selective heating of

nanoscale objects to dozens and hundreds of degrees Celsius. This effect is controlled by optical irradiation parameters and can be used to selectively affect a specific virus type among other viruses in a solution.

[1] H. K. Yadav, V. Gupta, K. Sreenivas, S. P. Singh, B. Sundarakannan, and R. S. Katiyar, Low Frequency Raman Scattering from Acoustic Phonons Confined in ZnO Nanoparticles, Phys. Rev. Lett. **97**, 085502 (2006).

[2] S. Wheaton, R. M. Gelfand, and R. Gordon, Probing the Raman-active acoustic vibrations of nanoparticles with extraordinary spectral resolution, Nat. Photon. **9**, 68 (2014).

[3] J. Burkhartsmeyer, Y. Wang, K. S. Wong, and R. Gordon, Optical trapping, sizing, and probing acoustic modes of a small virus, Appl. Sci. **10**, 394 (2020).

[4] N. V. Tcherniega, K. I. Zemskov, V. V. Savranskii, A. D. Kudryavtseva, A. Y. Olenin, and G. V. Lisichkin, Experimental observation of stimulated low-frequency Raman scattering in water suspensions of silver and gold nanoparticles, Opt. Lett. **38**, 824 (2013).

[5] J. Shi, H. Wu, J. Liu, S. Li, and X. He, Stimulated scattering effects in gold-nanorod-water samples pumped by 532 nm laser pulses, Sci. Rep. **5**, 11964 (2015).

[6] A. F. Bunkin, M. A. Davydov, A. N. Fedorov, V. N. Lednev, and S. M. Pershin, Anomalous stimulated Brillouin scattering in aqueous suspension of polystyrene nanospheres, Laser Phys. Lett. **16**, 015701 (2019).

[7] M. V. Arkhipenko, A. F. Bunkin, M. A. Davydov, O. V. Karpova, V. B. Oshurko, S. M. Pershin, V. N. Streltsov, and A. N. Fedorov, Stimulated low-frequency scattering of light in an aqueous suspension of the tobacco mosaic virus, JETP Lett. **109**, 578 (2019).

[8] R. El-Ganainy, D. N. Christodoulides, E. M. Wright, W. M. Lee, and K. Dholakia, Nonlinear optical dynamics in nonideal gases of interacting colloidal nanoparticles, Phys. Rev. A **80**, 053805 (2009).

[9] S. Li, G. Erdemci-Tandogan, J. Wagner, P. van der Schoot, and R. Zandi, Impact of a nonuniform charge distribution on virus assembly, Phys. Rev. E **96**, 022401 (2017).

[10] B. Michen and T. Graule, Isoelectric points of viruses, J. Appl. Microbiol. **109**, 388 (2010).

[11] S. Glasstone, Dispersion of conductance at high frequencies, *An Introduction to Electrochemistry* (Maurice, 2008), p. 101.

[12] M. Heyden, D. J. Tobias, and D. V. Matyushov, Terahertz absorption of dilute aqueous solutions, J. Chem. Phys. **137**, 235103 (2012).

[13] A. A. Andreev, *An Introduction to Hot Laser Plasma Physics* (Nova Science, Huntington, NY, 2012).

[14] M. V. Arkhipenko, A. F. Bunkin, M. A. Davydov, O. V. Karpova, V. B. Oshurko, S. M. Pershin, and A. N. Fedorov, Frequency shift of acoustic oscillations of the Tobacco Mosaic Virus with varying suspension parameters, Bull. Lebedev Phys. Inst. **45**, 334 (2018).

[15] A. F. Bunkin, M. A. Davydov, S. M. Pershin, N. V. Suyazov, and A. N. Fedorov, Low-frequency stimulated scattering in an aqueous suspension of dielectric nanospheres, Bull. Lebedev Phys. Inst. **46**, 243 (2019).

[16] B. Stephanidis, S. Adichtchev, P. Gouet, A. McPherson, and A. Mermet, Elastic properties of viruses, Biophys. J. **93**, 1354 (2007).

[17] N. A. Nikitin, I. N. Matveeva, E. A. Trifonova, N. M. Puhova, A. Y. Samuylenko, S. A. Gryn, J. G. Atabekov, and O. V. Karpova, Spherical particles derived from TMV virions enhance the protective properties of the rabies vaccine, Data in Brief **21**, 742 (2018).

[18] J. Atabekov, N. Nikitin, M. Arkhipenko, S. Chirkov, and O. Karpova, Thermal transition of native TMV and RNA-free viral proteins into spherical nanoparticles, J. Gen. Virol. **92**, 453 (2011).